Narrow $6p_{1/2,3/2}np$ $J=1$ autoionizing Rydberg series in barium and their interaction with $6p_{3/2}nf$ states

R. J. de Graaff, W. Ubachs, and W. Hogervorst
Laser Centre, Free University of Amsterdam, Faculteit Natuurkunde en Sterrenkunde, De Boelelaan 1081, 1081 HV Amsterdam, The Netherlands

M. Abutaleb
Department of Physics, Cairo University, Giza, Egypt
(Received 29 May 1990)

The $6p_{1/2,3/2}np$ and $6p_{3/2}nf$ ($J=1$) series in barium were excited in a two-step pulsed laser experiment starting on the $6s5d\ ^3D_1$ metastable state via the $5d6p\ ^3P_0$ as intermediate level. Use was made of the $6s_{1/2}6p_{1/2}$ character mixed into the $5d6p\ ^3P_0$ level to excite the $6pnp$ series, which appear to have extremely low autoionizing rates compared to other $6pnl$ series. The observed spectra were analyzed using a seven-channel multichannel quantum-defect theory analysis. Evidence of configuration interaction between the $6p_{1/2}np$ and $6p_{3/2}nf$ series was found.

I. INTRODUCTION

Studies of autoionization properties of doubly excited atomic states are greatly facilitated using multistep laser excitation. The $5dnl$ and $6pnl$ Rydberg series in barium were studied most extensively and autoionization rates for several angular momentum series converging to both $5d_j$ and $6p_j$ Ba^+-ion limits were determined recently.[1-9] For states with high orbital angular momentum l, having near-hydrogenic wave functions for the Rydberg electron with only a small overlap with the core electron, autoionization rates are low. Both Jones and Gallagher[5] and Poirier[10] performed calculations on the long-range interaction between the Rydberg and core electron and the resulting autoionization rates for $l>4$ agree well with observations on $6png$ (Ref. 8), $6pnh$ (Ref. 1), and $6pnl$ ($l\geq 4$) (Ref. 5) series in barium. Long-lived states at certain values of the principal quantum number n, may also result from a coincidental interference between different channels. This effect of inhibited autoionization can be parametrized and understood in the framework of multichannel quantum-defect theory (MQDT). An example is the $5d_{3/2}26d_{3/2}$ $J=0$ autoionizing resonance, for which a lifetime of 190 ns is reported.[11]

In this paper we present the observation of a different type of narrow autoionizing states. The $6pnp$ $J=1$ series has low angular momentum and therefore a large overlap in the wave functions of core and Rydberg electrons. For this reason a high autoionization rate for the series as a whole might be expected. However, although configuration interaction between the $6p_{1/2}np_{3/2}$ and the rapidly autoionizing $6p_{3/2}nf_{5/2}$ $J=1$ series occurs, the observed width of $6p_{1/2}np_{3/2}$ states turns out to be extremely narrow.

Experimentally we did not apply the isolated-core excitation (ICE) scheme[12] thus far mainly used for the investigation of $6pnl$ states. The ICE method, in which first a well-defined bound $6snl$ Rydberg state is prepared, followed in the next step by the $6s$-$6p$ core excitation, has the notable advantage of a large oscillator strength on the core transition. Nevertheless, we followed an alternative excitation procedure: preparation of a doubly excited $5d6p$ bound state followed by the excitation of the autoionizing $6pnp$ level. In contrast to the ICE scheme, where a spectrum has to be recorded for each individual n value, in our scheme the complete Rydberg series may be recorded in a continuous wavelength scan. This is a major advantage as the interactions between different channels, including continuum interactions, show at first glance in the recorded features as line shifts, Beutler-Fano profiles and, most important, in the oscillator strength distribution (dS/dE) over a large energy (E) range.

In the present experiment the doubly excited state $5d_{3/2}6p_{3/2}\ ^3P_0$ of barium was prepared as an intermediate level by one-photon absorption from the $6s5d\ ^3D_1$ metastable state. The $6pnp$-$6pnf$ $J=1$ spectrum was recorded by uv excitation in the wavelength range 260–280 nm. For $J=1$ four $6pnp$ Rydberg series exist, two converging to the $6p_{1/2}$ limit and two to the $6p_{3/2}$ limit. As only the $6p_{3/2}$ series can be excited from the $5d_{3/2}6p_{3/2}\ ^3P_0$ state, the $6s_{1/2}6p_{1/2}$ character, which is expected to be mixed into this state,[13,14] is required for the excitation of the $6p_{1/2}$ series. In addition, one $6p_{3/2}nf_{5/2}$ series (in jj-coupling notation) may be observed. The strict selection rules $\Delta J=+1$ and $\Delta l=\pm 1$, when starting from $^3P_0$, limits the excitation to the series mentioned, and all features observed are undoubtedly related to these mutually perturbing $J=1$ series. Excitation of $J\neq 1$ states, which complicated the study of Story, Yap, and Cooke[9] of unperturbed $6pnp$ series above the $6p_{1/2}$ limit, is excluded.

In the following sections first the experimental details are discussed, especially the suppression of background signal due to the direct uv ionization of metastables. Next the experimental results are presented and ana-

lyzed. Finally the results of a seven-channel phase-shifted R-matrix MQDT analysis will be given and discussed.

II. EXPERIMENTAL PROCEDURE

In the experimental setup, schematically shown in Fig. 1, two tunable dye lasers synchronously pumped by a neodymium-doped yttrium aluminum garnet (Nd:YAG) laser (DCR3-Quanta Ray) were used. A first dye laser, running on Rhodamine 640, was pumped by the 532-nm second-harmonic output of the Nd:YAG laser, while a second dye laser was pumped either by the 532-nm or by the 355-nm output of the Nd:YAG laser. Tunable radiation in the wavelength range $\lambda \sim 260-267$ nm, required for the excitation of $6p_{3/2}nf$ and $6p_{3/2}np$ states, was produced by 355-nm pumping of Coumarine dyes and frequency doubling in a beta-barium-borate (BBO) crystal. To excite the $6p_{1/2}np$ series the range $\lambda > 267$ nm was covered by 532-nm pumping of yellow and red dyes and subsequent doubling in a potassium dihydrogen phosphate (KDP) crystal. Typically uv powers of 1 mJ/pulse were used. The dye lasers had a linewidth of 0.3 cm^{-1} in the visible range and 0.45 cm^{-1} in the uv range after frequency doubling.

The barium atomic beam source was a small tantalum oven, heated by thermal radiation and electron bombardment from a resistively heated tungsten wire mounted in front of the oven orifice. Moreover, a low-voltage 800-mA discharge was maintained between the tungsten wire and the oven. In the resulting atomic beam, a fraction of the barium atoms was transferred to the $^1D_2$ and $^3D_{1,2,3}$ $6s5d$ metastable states (about 1% each).[13,15] The uv and visible pulsed laser beams perpendicularly cross the atomic beam from opposite sides between two capacitor plates. In the interaction region the laser pulses are temporally and spatially overlapped. By applying suitable voltages over the capacitor plates, photoelectrons can be prevented from reaching or can be accelerated through a series of grids onto an electron multiplier.

Figure 2 shows a schematic diagram of energy levels relevant for the excitation of $6p_{1/2,3/2}np,nf$ autoionizing series of barium in the present study. The figure shows the different ionization limits (excited states of Ba^+) by bold lines and the $6pnl$ series by thin lines. The two-step laser excitation is indicated by arrows. The first laser was tuned to resonance on the transition $6s5d\ ^3D_1 - 5d6p\ ^3P_0$ at $\lambda = 602$ nm by observing photoelectrons from $1+1$ multiphoton ionization on this transition. Next, the power of the first laser was lowered in such a way that the population of $5d6p\ ^3P_0$ was optimized while minimizing the production of electrons from this visible laser beam. Keeping the frequency of this laser constant, the second laser (uv) was scanned across the $5d6p$-$6pnp,nf$ of transitions, and electrons produced by autoionizing decay were detected as a function of uv wavelength.

The $6pnp$ and $6pnf$ $J=1$ spectra were obtained from detection of photoelectrons after autoionization into the $5d\epsilon l$ and/or $6s\epsilon l$ continua. With equal voltages V_1 and V_2 on the capacitor (see Fig. 1) the autoionizing states were excited in a field-free region. A major experimental problem was the necessary reduction of background electrons produced in several competing photoionization processes. Electrons emitted from the autoionization process of the $6pnl$ series into the $5d$ and $6s$ continua have an energy of 2–3 eV. The large numbers of low-energy electrons (1–2 eV), produced in direct uv photoionization from metastable states, were effectively suppressed by introducing a repelling voltage of about 3 V on the grid V_3 which, because of low resolution, selected mainly electrons with an energy larger than 2 eV. The set of plates V_1, V_2, and V_3 was set at a negative voltage of -100 V with respect to the grounded first dynode of the electron multiplier, such that all charged particles passing V_3 were accelerated and detected. In this arrangement the low-energy electrons produced in the excitation of a

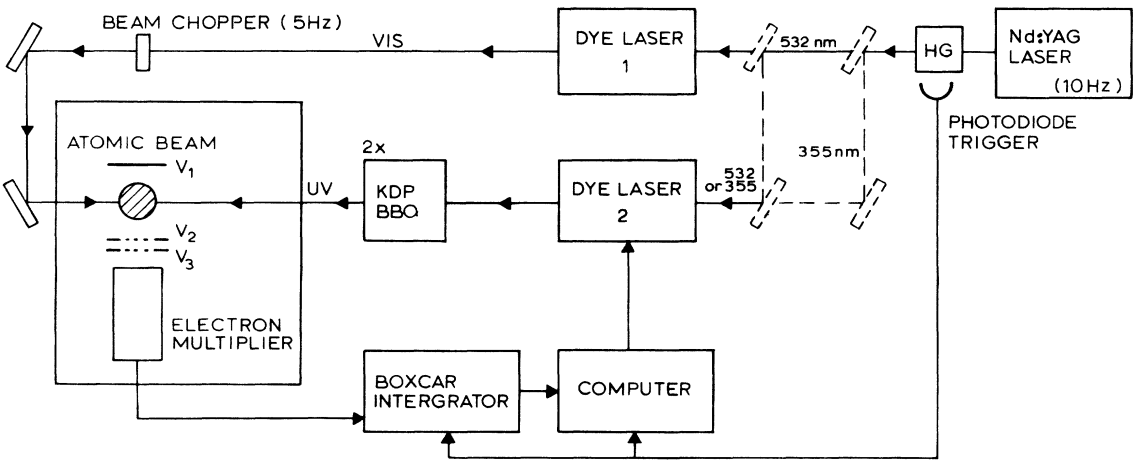

FIG. 1. Schematic of the experimental setup (HG denotes harmonic generator).

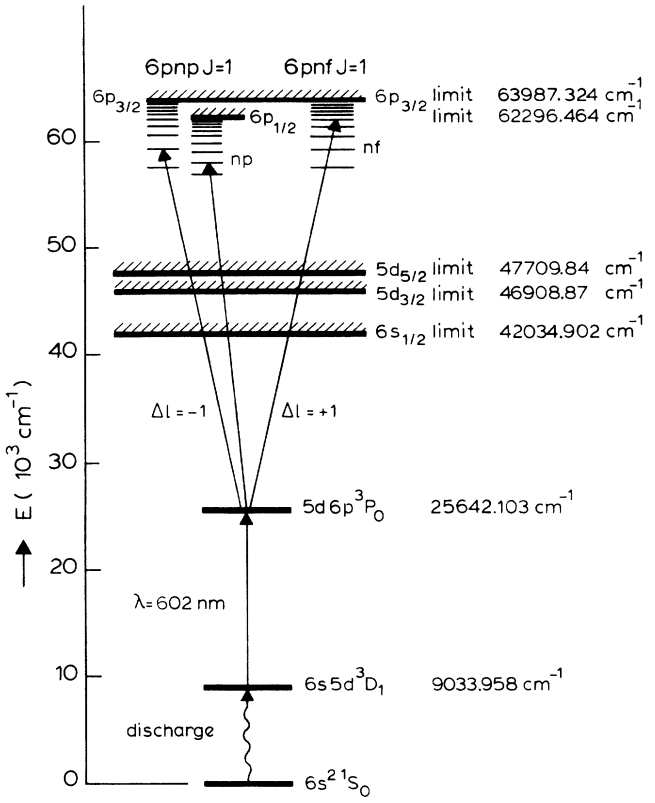

FIG. 2. Energy-level diagram showing the excitation scheme.

$6p_{3/2}nl$ state followed by autoionization into the $6p_{1/2}$ channel of Ba^+ could not be observed. Furthermore, a beamstop was moved in and out of the visible laser beam at half the repetition frequency of the laser and the single-shot information was alternatingly stored in two input channels of the computer. In this way the remaining uv-induced background spectrum could be subtracted from the 1 visible $+1$ uv multiphoton spectrum, thereby efficiently increasing the signal-to-noise ratio in the $6pnp$-$6pnf$ spectra. At each wavelength setting of the dye laser, signals were summed over 12 laser shots.

The uv spectrum in one of the input channels contained also information on the one-photon excitation from the $6s^2$ ground state to mainly $6snp$ $J=1$ states followed by photoionization of these states. This process produces 4-eV electrons. These lines[16] were used for wavelength calibration. The accuracy in the determination of the frequency position of $6pnp$ Rydberg features is about 0.3 cm^{-1}, mainly due to small nonlinearities in the scans.

III. RESULTS AND INTERPRETATION

In the frequency domain between the $6p_{3/2}$- and $6p_{1/2}$-ionization limits, at 63 987.324 and 62 296.464 cm^{-1}, respectively, a single unperturbed autoionizing Rydberg series was observed. In the one-photon absorption from the $5d6p\ ^3P_0$ intermediate level (at 25 642.103 cm^{-1}) only transitions with $\Delta J=+1$ are allowed and for those the transitions with $\Delta l=+1$ are expected to be strongest. Indeed, in the range above the $6p_{1/2}$ limit, only the $6p_{3/2}nf_{5/2}$ $J=1$ states, with quantum defect $\delta_f=0.08$ appeared, and no additional features due to $6p_{3/2}np$ $J=1$ states were observed.

The $6p_{3/2}8f_{5/2}$ $J=1$ autoionizing resonance lies at 62 190 cm^{-1}. Because of its large width [150 cm^{-1} full width at half maximum (FWHM)] this broad feature extends over the $6p_{1/2}$ ionization limit. Superimposed on it is a long regular double progression of narrow resonances converging to this $6p_{1/2}$ limit. One of these two series in the experimental spectrum of Fig. 3 shows very narrow linewidths (for high n laser linewidth), while the other is much broader and lines are shaped according to the Beutler-Fano profiles. This double progression shows members of the $6p_{1/2}np_{1/2}$ and $6p_{1/2}np_{3/2}$ Rydberg series (in the jj-coupling scheme). At lower energy around 61 700 cm^{-1} the double $6p_{1/2}np$ series interacts with the broad $6p_{3/2}7f_{5/2}$ feature. However, for $n=17$–20 the two $6p_{1/2}np$ series are more strongly perturbed than in the range of $6p_{3/2}8f_{5/2}$. At $n=19$, triplets instead of doublets appear (see Fig. 3), thus suggesting perturbing interactions with $6p_{3/2}np$ states.

To gain more insight in this $6p_{1/2}np$-$6p_{3/2}np$ series interaction, quantum defects of the $6pnp$ features with respect to the lower $6p_{1/2}$ ionization limit were plotted in a Lu-Fano plot as a function of the effective quantum number ν with respect to the $6p_{3/2}$ limit, as shown in Fig. 4. These quantum defects were deduced from a fit of individual resonances to Lorentz or Fano profiles resulting in the energy values E_{obs} given in Table I. The energy values for those features fitted with Fano profiles are not reliable as the precise positions of the maxima in oscillator strength within a series have to follow from an MQDT analysis (Sec. IV). Energy positions for the $6p_{1/2}17p$ and $6p_{1/2}18p$ states are not given in Table I, as for these states interaction with the broad $6p_{3/2}7f$ state results in strongly asymmetric line profiles. Furthermore, it is important to note that interactions between $6p_{1/2}np$ and $6p_{3/2}nf$ series as well as interactions with continua distort a two-dimensional Lu-Fano plot. This partly explains the deviations between experimental points and calculated curves in Fig. 4 (these curves are derived from a limited four-channel bound MQDT analysis). Nevertheless, the Lu-Fano plot clearly shows how the two $6p_{1/2}np$ series with reduced quantum defects of -0.13 (quantum defect $\delta_1=3.87$) and -0.22 ($\delta_2=3.78$) are perturbed by two states with approximate reduced quantum defects with respect to the upper limit $6p_{3/2}$ of -0.10 and -0.23. From this result we derive the quantum defects for the $6p_{3/2}np$ series to be $\delta_3=3.90$ and $\delta_4=3.77$. Strictly, the Lu-Fano treatment only yields quantum-defects modulus 1. The real values of the quantum defects were obtained from an extrapolation to the bound $6p^2$ $J=1$ state at 34 823 cm^{-1}.[17] Thus we find that the strong perturbation near 61 850 cm^{-1} is due to two $6p_{3/2}11p$ states, interacting strongly with the $6p_{1/2}19p$ and $6p_{1/2}20p$ states.

As discussed before, the $6p_{3/2}np$ series above the $6p_{1/2}$

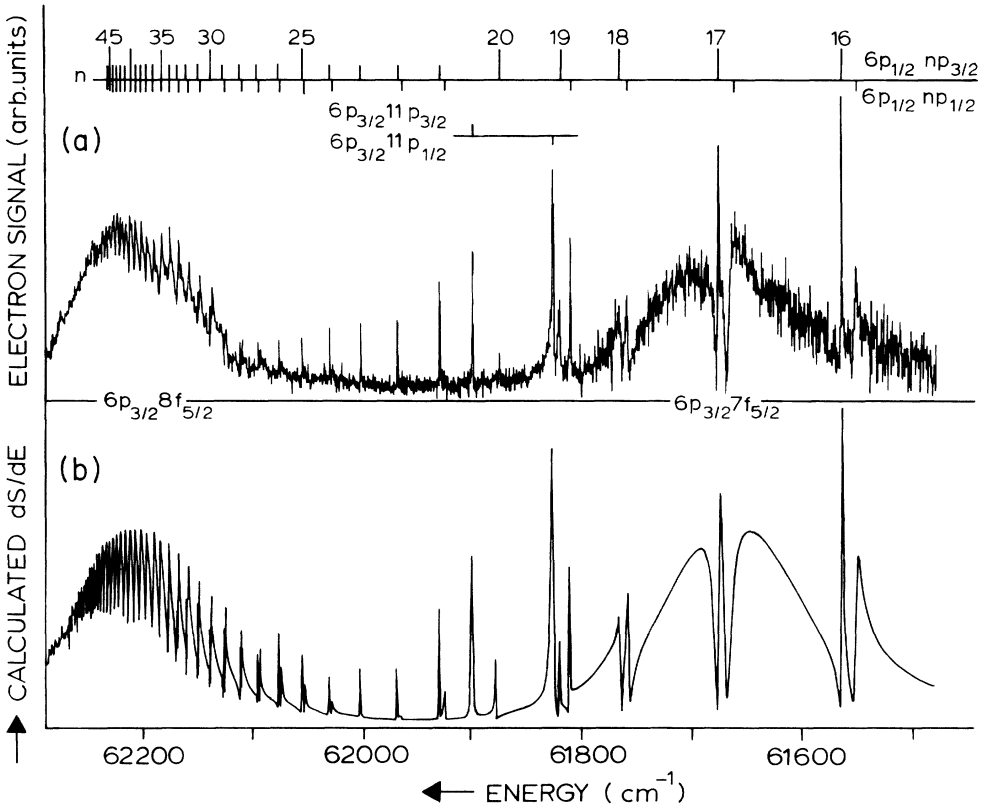

FIG. 3. (a) Observed spectrum of the $6p_{1/2}np\ J=1$ ($n>16$) series with the $6p_{3/2}7f$, $6p_{3/2}8f$, and $6p_{3/2}11p$ perturber states. (b) Calculated oscillator strength distribution dS/dE resulting from the seven-channel MQDT fit.

limit could not be observed using the excitation scheme with the $5d6p\ ^3P_0$ intermediate states. However, by tuning the first laser to $\lambda\sim 653$ nm, the $5d6p\ ^3D_2$ state could be prepared as an intermediate state by excitation from the $6s5d\ ^3D_2$ metastable level. Scanning the second uv laser then yields strong and broad features of an autoionizing $6p_{3/2}nf\ J=3$ series and several narrower, less intense lines identified as $6pnp\ J=1$ resonances. Starting from $5d6p\ ^3D_2$, the $6pnp$ states with a total angular momentum $J=1$ are favored in the excitation ($\Delta l=-1$ and $\Delta J=-1$). The resulting positions of $6p_{3/2}np\ J=1$ states, which are not perturbed by the $6pnf\ J=3$ series also observed, are included in Table I. The quantum defects agree well with the values derived from the Lu-Fano plot analysis, as discussed above.

An indication for the assignment of the four $6p_{1/2,3/2}np_{1/2,3/2}\ J=1$ autoionizing series can be deduced from a calculation of the energy splittings within the configuration due to monopole and quadrupole electrostatic interactions (direct and exchange) and spin-orbit interactions of core and Rydberg electron. Taking the values of Story *et al.*[9] for the electrostatic interaction, diagonal in LS coupling, and the spin-orbit interaction diagonal on a jj basis, the energy matrix elements of $T'_{jj\to LS}H_{\rm es}T_{LS\to jj}+H_{\rm s.o.}$ were evaluated. The matrix T denotes the LS-jj transformation matrix. The 4×4 ma-

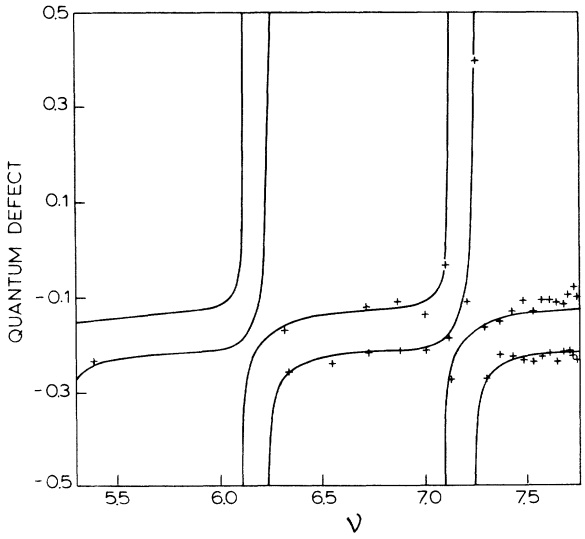

FIG. 4. Quantum-defect plot of the $6pnp\ J=1$ series, excluding $6pnf$ perturbers. +, represents experimental points; the lines drawn are from a limited four-channel MQDT analysis.

trix was diagonalized and the four resulting eigenvalues correspond to jj-coupled states for $J=1$ in the order of highest to lowest energy: $6p_{3/2}np_{3/2}$, $6p_{3/2}np_{1/2}$, $6p_{1/2}np_{3/2}$, $6p_{1/2}np_{1/2}$. The calculated splittings using the interaction parameters of Story *et al.*[9] agree reasonably well with the observed splittings. Away from the strong $6p_{1/2}19p$-$6p_{3/2}11p$ perturbation, this calculation allows for an unambiguous assignment of spectral lines as $|jj'\rangle$ states.

Contrary to common practice, the widths of the autoionizing resonances are not listed in Table I. The $6p_{1/2}np_{1/2}$ resonances are far from symmetric because of a strong interaction with $6pnf$ and the underlying continuum. The spectral width of the narrow $6p_{1/2}np_{3/2}$ series at higher n is determined by the bandwidth of the exciting uv laser. To increase the accuracy in the determination of the scaled linewidth of this narrow $6p_{1/2}np_{3/2}$ $J=1$ series, the $6p_{1/2}11p_{3/2}$ resonance was investigated (see Fig. 5). This state is located at 60 199.7 cm^{-1}, in between but far away from the $6p7f$ and $6p6f$ perturbers.

TABLE I. Level energies (E_{obs}) and effective quantum numbers (ν) of the $6pnp$ $J=1$ states measured in transitions from the $5d6p\ ^3P_0$ intermediate state as deduced from fits to Lorentz or Fano profiles (marked with asterisks) and deviations from calculated energies (E_{calc}) using a seven-channel MQDT model. Energy positions of resonances marked with asterisks were calculated from maxima in the oscillator strength distribution of the designated channel only.

Label	ν	E_{obs} (cm^{-1})	$E_{obs}-E_{calc}$ (cm^{-1})
$6p_{1/2}11p_{3/2}$	7.241	60 199.7	−0.2
$6p_{1/2}14p_{3/2}$	10.256	61 254.0	1.0
$6p_{1/2}15p_{3/2}$	11.226	61 428.0	−3.4[a]
$6p_{1/2}16p_{1/2}$*	12.131	61 549.9	0.0
$6p_{1/2}16p_{3/2}$*	12.220	61 561.6	1.0
$6p_{1/2}19p_{1/2}$	15.025	61 811.1	−0.1
$6p_{1/2}19p_{3/2}$	15.180	61 820.8	−0.2
$6p_{3/2}11p_{1/2}$	15.252	61 826.2	−0.3
$6p_{1/2}20p_{1/2}$*	16.068	61 873.8	2.0[a]
$6p_{3/2}11p_{3/2}$	16.616	61 898.6	0.0
$6p_{1/2}21p_{1/2}$	17.160	61 924.1	−0.5
$6p_{1/2}21p_{3/2}$	17.282	61 928.7	−0.6
$6p_{1/2}22p_{3/2}$	18.244	61 966.1	−0.6
$6p_{1/2}23p_{1/2}$	19.143	61 996.7	0.0
$6p_{1/2}23p_{3/2}$	19.234	61 999.7	0.0
$6p_{1/2}24p_{1/2}$*	20.140	62 025.1	−0.7
$6p_{1/2}24p_{3/2}$	20.229	62 028.5	−0.3
$6p_{1/2}25p_{1/2}$*	21.137	62 050.8	0.1
$6p_{1/2}25p_{3/2}$	21.227	62 053.2	0.5
$6p_{1/2}26p_{1/2}$*	22.136	62 072.0	0.3
$6p_{1/2}26p_{3/2}$	22.225	62 074.4	0.2
$6p_{1/2}27p_{1/2}$*	23.135	62 091.0	−0.2
$6p_{1/2}27p_{3/2}$	23.223	62 093.0	0.1
$6p_{1/2}28p_{1/2}$*	24.133	62 107.8	−0.1
$6p_{1/2}28p_{3/2}$	24.222	62 109.7	0.4
$6p_{1/2}29p_{1/2}$*	25.132	62 122.5	−0.2
$6p_{1/2}29p_{3/2}$	25.221	62 123.9	0.1
$6p_{1/2}30p_{1/2}$*	26.132	62 135.4	−0.1
$6p_{1/2}30p_{3/2}$	26.220	62 136.8	0.1
$6p_{1/2}31p_{1/2}$*	27.131	62 146.9	−0.3
$6p_{1/2}31p_{3/2}$	27.220	62 148.5	0.2
$6p_{1/2}32p_{1/2}$*	28.130	62 157.8	0.2
$6p_{1/2}32p_{3/2}$	28.219	62 158.8	0.2
$6p_{1/2}33p_{1/2}$*	29.107	62 166.9	0.1
$6p_{1/2}33p_{3/2}$	29.253	62 168.2	0.4
$6p_{1/2}34p_{1/2}$*	30.091	62 175.3	0.0
$6p_{1/2}34p_{3/2}$	30.268	62 176.7	0.4
$6p_{3/2}18p_{3/2}$	14.215	63 444.2	0.0[b]
$6p_{3/2}20p_{3/2}$	16.214	63 570.0	0.2[b]
$6p_{3/2}21p_{3/2}$	17.213	63 616.9	0.3[b]
$6p_{3/2}22p_{3/2}$	18.213	63 656.8	0.1[b]
$6p_{3/2}23p_{3/2}$	19.213	63 691.0	0.7[b]

[a]Weak, heavily perturbed states.

[b]Levels observed in excitation from the $5d6p\ ^3D_2$ intermediate state (experimental accuracy in these lines is $\pm 1\ cm^{-1}$).

IV. MQDT ANALYSIS

Multichannel quantum-defect theory has proven to be a powerful tool for analyzing interactions between atomic Rydberg series with the same angular momentum J and parity. In its early stage of development, quantum-defect theory was mainly applied to problems of bound Rydberg series interacting with localized doubly excited states below the first ionization limit.[18] Today the "phase-shifted reaction matrix" MQDT formalism, as presented by Cooke and Cromer[19] and Giusti-Suzor and Fano,[20] is preferentially used for the analysis of interactions between autoionizing series and various continua. The phase-shifted formalism has the notable advantage that it

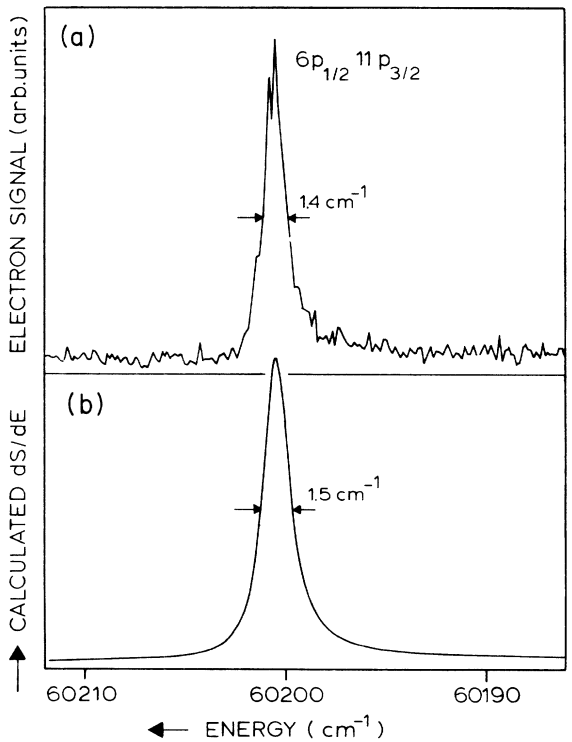

FIG. 5. (a) Experimental excitation profile of the $6p_{1/2}11p_{3/2}$ state. (b) Calculated profile from the MQDT fit.

that it is applicable even under circumstances where the angular momentum coupling does not change from *jj* coupling in the outer Coulomb region (collision channel) to mainly *LS* coupling close to the core (close-coupling channel). This is found to be the case for the doubly excited series in barium. Another important advantage of this formalism is that it allows for a stepwise analysis of the experimental data. In a first step a few selected bound (closed) channels are analyzed. Next, the other bound channels and eventually the continuum (open) channels are added. The present data were analyzed within the framework of this "phase-shifted reaction matrix" formalism. This MQDT model is described elsewhere in detail, so we only will summarize those aspects, which are relevant for the interpretation of the result of our MQDT fit. For further details we refer to earlier papers.[19,21–23]

The channel wave functions are defined at large radius r where the Rydberg wave function is separable into a radial and an angular part and has a well-defined ion core. The basic matrix equation to be solved is given by

$$[\underline{R}'+\tan(\pi\nu')]\mathbf{a}'=\mathbf{0}\ , \tag{1}$$

where $\nu_i'=\nu_i+\delta_i$, and ν_i represents the effective quantum number of a given energy with respect to the ionization limit belonging to channel i. The symmetric matrix $\underline{R}'$ has only off-diagonal elements, which represent the channel interactions independent of the single-channel quantum-defect δ_i. This is the quantum defect belonging to a certain channel i in the absence of interactions. Using the pseudoeigenvector $\mathbf{a}'$ and the dipole moment parameters D_i' of the phase-shifted channels the oscillator strength distribution dS/dE can be calculated[23] according to

$$\frac{dS}{dE}=\left[\sum_{\{n_c\}}\sum_{i}a_i'D_i'\right]^2 . \tag{2}$$

Here n_c represents the number of open channels. For a single channel (i) (or states belonging to a channel in a region where the channel mixing is weak) interacting with a single continuum (j) in case of only weak direct excitation of the continuum, the scaled linewidth ($\nu_i^3\Gamma$) at full width at half maximum in atomic units is given by

$$\nu_i^3\Gamma=\frac{2R_{ij}^2}{\pi}\ . \tag{3}$$

The MQDT analysis was executed in four steps, each consecutive step dealing with more complex parts of the spectrum. Firstly, the single $6p_{3/2}nf$ and $6p_{3/2}np$ $J=1$ series above the $6p_{1/2}$ limit were parametrized. These are, in principle two-channel problems, with one closed channel (the $6pnf$ or $6pnp$ series) interacting with one open channel representing the different continua involved. Secondly, from the Lu-Fano plot shown in Fig. 4, starting values for the quantum defects of the $6p_{1/2}np$ series and their interaction with the $6p_{3/2}n'p$ series (for $n=19$–22 and $n'=11$) were deduced and used as starting values for a fit to this part of the spectrum in a four-channel MQDT analysis. Thirdly, the complete spectrum was considered in a seven-channel analysis using the results from preceding steps as input. Further optimization of the parameters on the basis of trial and error resulted in a calculated spectrum which reproduced all relevant experimental features. Finally, a direct fit to the observed spectrum was performed using a Levenberg-Marquardt algorithm as implemented by Moré *et al.*[24]

Our analysis aimed at a maximum reduction of data by keeping the number of parameters as low as possible. The reaction matrix elements were taken to be independent of energy, while all four $6pnp$ series (channels 1–4) were assumed to interact only with a single continuum (channel 6). Interactions between $6pnp$ series converging to a common limit were not considered. The second continuum (channel 7) only interacts with the $6pnf$ series (channel 5); continuum-continuum interactions were ignored. The even parity $6pnp$ and $6pnf$ $J=1$ states below the $6p_{1/2}$ limit may autoionize into the following continua: $6s_{1/2}\epsilon s_{1/2}$, $6s_{1/2}\epsilon d_{3/2}$, $5d_{3/2}\epsilon s_{1/2}$, $5d_{3/2}\epsilon d_{3/2}$, $5d_{3/2}\epsilon d_{5/2}$, $5d_{5/2}\epsilon d_{3/2}$, $5d_{5/2}\epsilon d_{5/2}$, and $5d_{5/2}\epsilon g_{7/2}$. The series observed above the $6p_{1/2}$ limit, apart from the two $6s\epsilon l$ and the six $5d\epsilon l'$ channels, have also two $6p_{1/2}\epsilon l''$ autoionization channels available. For the analysis below the $6p_{1/2}$ limit we chose for the decay of the $6pnp$ series one of the $6s\epsilon l$ continua and for the decay of the $6p_{3/2}nf$ series one of the $5d\epsilon l'$ continua. However, the selection and number of continua (provided larger than two) did not really seem to affect the fit.

The results of the MQDT analysis are presented in Tables I and II and in Fig. 3, where the spectrum (b) generated with the obtained MQDT parameters is plotted below the observed spectrum (a). It should be noted that the calculated spectrum as convoluted with a linewidth of 0.45 cm^{-1}, corresponding to the bandwidth of the uv laser. Table I lists the observed peak positions E_{obs} for the $6pnp$ $J=1$ lines and deviations from calculated values ($E_{obs}-E_{calc}$) using the seven-channel MQDT fit. For the resonances analyzed with Fano profiles, E_{calc} gives the maxima in the oscillator strength distribution calculation, where in Eq. (2), instead of the summation over all channels, the term belonging to the designated channel was taken. The $6p_{3/2}np$ features observed in the excitation scheme using the $5d6p\ ^3D_2$ intermediate state are included as well. In Table II the optimized MQDT parameters are presented. The errors given to those parameters which were optimized are derived from the covariance matrix of the fitting procedure by multiplying the square root of the diagonal elements with a noise factor, determined by the noise distribution in the spectra.

V. DISCUSSION

As is evident from Fig. 3, the major characteristics of the experimental spectrum, noteworthily the oscillator strength distribution, could be reproduced using a seven-channel MQDT model with the simplifying assumptions discussed in Sec. IV. Energy-level positions were fitted satisfactorily apart from two resonances marked with superscript a in Table I, having low weight in the fit due to their small oscillator strengths and narrow widths. Di-

TABLE II. MQDT parameters for the $6pnf$ and $6pnp$ $J=1$ series in a seven-channel analysis. The index i denotes the channels, I_i the ionization limits, δ_i the quantum defects with energy dependence $d\delta_i$, and D_i the dipole moment of the excitation channel. Errors are determined by the covariance matrix from the fit and the noise in the spectra (see text) and correspond with one standard deviation.

	$i=1$ $6p_{1/2}np_{1/2}$	$i=2$ $6p_{1/2}np_{3/2}$	$i=3$ $6p_{3/2}np_{1/2}$	$i=4$ $6p_{3/2}np_{3/2}$	$i=5$ $6p_{3/2}nf_{5/2}$	$i=6$ continuum 1	$i=7$ continuum 2
I_i	62 296.46	62 296.46	63 987.32	63 987.32	63 987.32	42 034.90	46 908.75
δ_i	3.87(1)	3.781(3)	3.889(3)	3.756(2)	0.08(1)		
$d\delta_i$	0.20(1)	0.20(1)	−0.2	−0.03	−0.4		
D_i	−0.3(3)	−0.5(2)	0.8(3)	0.4(4)	5(1)	0.0(2)	0.0(2)
				$\underline{R}$ matrix			
	1	2	3	4	5	6	7
1							
2	0						
3	−0.11(1)	−0.02(1)					
4	−0.17(2)	0.17(1)	0				
5	−0.20(5)	−0.11(4)	0	0			
6	−0.2(1)	−0.08(2)	−0.05(2)	0.05(3)	0		
7	0	0	0	0	0.58(4)	0	

pole moments for the $6s_{1/2}6p_{1/2}\,{}^3P_0 \rightarrow 6p_{1/2}np_{1/2,3/2}$ $(J=1)$, $5d_{3/2}6p_{3/2}\,{}^3P_0 \rightarrow 6p_{3/2}np_{1/2,3/2}$ $(J=1)$, and $5d_{3/2}6p_{3/2}\,{}^3P_0 \rightarrow 6p_{3/2}nf_{3/2}$ $(J=1)$ transitions were calculated with Racah algebra, assuming jj coupling for the $6pnp$ series. A comparison of these dipole moments with the moments given by the MQDT analysis yields an estimate of the admixture of $6s_{1/2}6p_{1/2}\,{}^3P_0$ character into the $5d_{3/2}6p_{3/2}\,{}^3P_0$ state. This turns out to be 1.5(1.0)%. slightly larger than a prediction (0.6%) from an earlier MQDT analysis of the interaction between the $6snp$ series and the $5d8p$ level.[13] A strong nonlinear energy dependence had to be incorporated to reproduce the position of the lower-lying $5d7p$ and $5d6p$ states, which is an indication of electron correlation effects. These electron correlations were also predicted by Grundevik *et al.*[14] for the $5d6p$ states.

The autoionization widths are determined by the reaction matrix elements R'_{61}, R'_{62}, R'_{63}, R'_{64}, and R'_{75} for the $6p_{1/2,3/2}np_{1/2,3/2}$ and $6p_{3/2}nf_{3/2}$ channels, respectively. Figure 5(b) shows the calculated profile for the $6p_{1/2}11p_{3/2}$ resonance, using the fit results for these matrix elements. The scaled autoionizing widths then follow from Eq. (3). The results are tabulated in Table III together with other published data on scaled linewidths for the $6pnl$ $(J=1)$ series. It is remarkable that the linewidths of the $6p_{1/2}np_{3/2}$, $6p_{3/2}np_{1/2}$, and $6p_{3/2}np_{3/2}$ $(J=1)$ channels are an order of a magnitude smaller than the values reported for the $6p_{1/2}np$ $(J=2)$ and $6p_{3/2}np$ $(J=3)$ series[1] and by far the smallest up to $l=6$. Thus far this effect has not been explained satisfactorily. Possibly a cancellation in the contribution of direct and exchange autoionization amplitudes occurs. Only *ab initio* calculations can validate this assumption. The covariance matrix gives a large error for R'_{61}, which can easily be understood. The $6p_{1/2}np_{1/2}$ channel is only excited near $6p_{3/2}np$ and $6p_{3/2}nf$ perturber states, clearly influencing the linewidths of the $6p_{1/2}np_{1/2}$ states, resulting in a large uncertainty in the determination of the scaled linewidth. In fact, it is possible that this series is even narrower than the other $6pnp$ series. This is currently under investigation in a cw laser experiment in our laboratory.

The observed linewidth FWHM for the $6p_{3/2}nf$ $(J=1$ series above the $6p_{1/2}$ limit (0.28 hartree) is of the same order of magnitude as the reported value for $6p_{3/2}nf$ $(J=3,4)$.[1,4] Analysis of the $6p_{3/2}nf$ $(J=1)$ series below the $6p_{1/2}$ limit using Eq. (3) results in a scaled linewidth of 0.21 hartree. This yields a branching ratio of about 25(10)% for decay of this series above the $6p_{1/2}$ limit into

TABLE III. Scaled total decay rates (Γ is FWHM) of Ba $6pnl$ with $J=1$ series and of Ba $6pnp$ series with $J=0$–3 in atomic units (hartree). Values in parentheses denote reported errors.

Label	J	$\nu^3\Gamma$ (hartree)	Reference
$6p_{1/2}ns_{1/2}$	0	0.11(2)	11
$6p_{3/2}np_{3/2}$	0	0.23(3)	9 (above $6p_{1/2}$ limit)
$6p_{1/2}np_{1/2}$	1	0.025(20)	This work
$6p_{1/2}np_{3/2}$	1	0.004(2)	This work
$6p_{3/2}np_{1/2}$	1	0.0016(10)	This work
$6p_{3/2}np_{1/2}$	1	0.035(7)	9 (above $6p_{1/2}$ limit)
$6p_{3/2}np_{3/2}$	1	0.002(2)	This work
$6p_{1/2}np$	2	0.06(2)	1
$6p_{3/2}np$	2	0.08(1)	9 (above $6p_{1/2}$ limit)
$6p_{3/2}np$	2	0.03(1)	9 (above $6p_{1/2}$ limit)
$6p_{3/2}np$	3	0.03(1)	1
$6p_{1/2}nf$	3,4	0.3(1)	1
$6p_{3/2}nf$	3,4	0.19(3)	1
$6p_{1/2}ng$	4	0.03	5
$6p_{1/2}nh$	5	$<0.009(2)$	1
$6p_{1/2}nh$	5	0.005	5
$6p_{3/2}nh$	5,4	$<0.008(3)$	1
$6p_{1/2}ni$	6	0.001	5

the $6p_{1/2}\epsilon l$ continua with respect to the decay into $6s\epsilon l$ and $5d\epsilon l$ continua. The reaction matrix elements R'_{51} and R'_{52} determine the configuration interaction between the $6p_{3/2}nf$ ($J=1$) and the $6p_{1/2}np$ channels. Above the $6p_{1/2}$ limit the same elements determine the widths due to autoionization into the $6p_{1/2}\epsilon p$ continua, resulting in a branching ratio of about 15(9)%. Hampered by a low signal-to-noise ratio, we were only able to determine the energy positions of the $6p_{3/2}np_{3/2}$ series, but not their linewidths. Our MQDT analysis, however, gives, by the same argument as above, but using R'_{41} and R'_{42}, a branching ratio of 94(5)%. The matrix elements R'_{31} and R'_{32} give a branching ratio of 81(14)% for the $6p_{3/2}np_{1/2}$ channel, which is more or less consistent with the value reported by Story *et al.* [67(5)%].[9] However, the calculated scaled linewidth [0.007(4) hartree] using the reported value of 67(5)% for the branching ratio is not consistent since these authors report a linewidth of 0.03(7) hartree, possibly indicating line broadening in their experiment. The MQDT analysis provides strong evidence for a considerable configuration interaction between the $6p_{3/2}nf$ channel and the two $6p_{1/2}np$ channels, as well as for channel interaction between the $6p_{3/2}np$ and $6p_{1/2}np$ channels.

VI. CONCLUSIONS

In this paper, observations of extremely narrow $6p_jnp_j$ ($J=1$) series interacting with a $6p_{3/2}nf$ ($J=1$) series excited from the bound $5d6p\ ^3P_0$ state were presented. We have reproduced the complete spectrum using a seven-channel MQDT fit. The channels could be identified by calculating the energy splitting due to electrostatic interactions. From the MQDT fit, configuration mixing coefficients and branching ratios could be deduced. The fact that we excited the $5d$ electron to a Rydberg state resulted in advantages over the commonly used isolated-core-excitation scheme, such as the unsaturated measurement of autoionization linewidths and the direct observation of the oscillator strength distribution.

ACKNOWLEDGMENTS

The authors wish to thank E. Bente for stimulating discussions and J. Bouma for his assistance during the experiment. They gratefully acknowledge financial support from the Foundation for Fundamental Research on Matter (FOM) and the Netherlands Organization for the Advancement of Research (NWO).

[1]E. Bente and W. Hogervorst, J. Phys. B **23**, 1403 (1990).
[2]C. J. Dai, S. M. Jaffe, and T. F. Gallagher, J. Opt. Soc. Am. B **6**, 1486 (1989).
[3]S. M. Jaffe, R. Kachru, H. B. van Linden, van den Heuvel, and T. F. Gallagher, Phys. Rev. A **32**, 1480 (1985).
[4]R. R. Jones, C. J. Dai, and T. F. Gallagher, Phys. Rev. A **41**, 316 (1990).
[5]R. R. Jones and T. F. Gallagher, Phys. Rev. A **38**, 2846 (1988).
[6]F. Gounand, T. F. Gallagher, W. Sandner, K. A. Safinya, and R. Kachru, Phys. Rev. A **27**, 1925 (1983).
[7]O. C. Mullins, Y. Zhu, E. Y. Xu, and T. F. Gallagher, Phys. Rev. A **32**, 2234 (1985).
[8]R. Kachru, H. B. van Linden, van den Heuvel, and T. F. Gallagher, Phys. Rev. A **31**, 700 (1985).
[9]J. G. Story, E. G. Yap, and W. E. Cooke, Phys. Rev. A **39**, 5127 (1989).
[10]M. Poirier, Phys. Rev. A **38**, 3484 (1988).
[11]L. D. v. Woerkom, J. G. Story, and W. E. Cooke, Phys. Rev. A **34**, 3457 (1986).
[12]W. E. Cooke and T. F. Gallagher, Phys. Rev. Lett. **41**, 1648 (1978).
[13]B. Post, W. Vassen, W. Hogervorst, M. Aymar, and O. Robaux, J. Phys. B **18**, 187 (1985).
[14]P. Grundevik, M. Gustavsson, G. Olsson, and T. Olsson, Z. Phys. A **312**, 1 (1983).
[15]W. Vassen, E. A. J. M. Bente, and W. Hogervorst, J. Phys. B **19**, 511 (1986).
[16]J. A. Armstrong, P. Esherick and J. J. Wynne, Phys. Rev. A **15**, 180 (1977).
[17]C. E. Moore, *Atomic Energy Levels,* Natl. Bur. Stand. Ref. Data Ser., Natl. Bur. Stand. (U.S.) Circ. No. 467 (U.S. GPO, Washington, D.C., 1971), Vol. III.
[18]M. Aymar, Phys. Rep. **110**, 163 (1984).
[19]W. E. Cooke and C. L. Cromer, Phys. Rev. A **32**, 2725 (1985).
[20]A. Giusti-Suzor and U. Fano, J. Phys. B **17**, 215 (1984).
[21]E. Bente and W. Hogervorst, Phys. Rev. A **36**, 51 (1987).
[22]E. Bente and W. Hogervorst, Z. Phys. D **14**, 119 (1989).
[23]A. Giusti-Suzor and H. Lefebvre-Brion, Phys. Rev. A **30**, 3057 (1984).
[24]J. J. Moré, B. S. Garbow, and K. E. Hillstrom, Argonne National Laboratory, Report No. ANL-80-74, 1980 (unpublished).